Electronic, Magnetic and Optical Properties of Transition Metal Doped Nd_2O_3: A DFT Insight

Priyanka Banerjee
Kazi Nazrul University
Kausik Mukhopadhyay (kausik_city@yahoo.com)
City College Kolkata https://orcid.org/0000-0002-7629-3378

Research Article

Keywords: Electronic Structure, Rare Earth Sesquioxide, Density Functional Theory, Fermi Energy, Band Structure Calculations, First-principles

Posted Date: January 12th, 2022

DOI: https://doi.org/10.21203/rs.3.rs-1216994/v1

Abstract

The structural, electronic, magnetic and optical properties of transition metal doped rare earth neodymium sesquioxide (Nd_2XO_3, where X = Co, Cr, Mn, Ni and Zn) was investigated here by first-principles simulations considering the density functional theory (DFT) framework. Comparing with the energy band structures, density of states and the overall charge density distribution, we find that the transition metal doping improves the application of the Nd_2O_3 (NDO) in many technological aspects. Spin-polarized calculations are quite satisfactorily described, and from this theoretical interpretation using DFT we fruitfully explain the mechanism behind the magnetic behavior of all doped samples. Electronic and optical properties of doped NDO samples are well tuned by transition metal atoms. Finally, we have seen that the values of total magnetization of transition metal substituted NDO samples are substantially enhanced compared to that of pure NDO.

1. Introduction

Rare-earth (RE) oxides and sesquioxides are now-a-days an interesting area of research for their significant applications in numerous electronic industries. Within the field of nanoscience and nanotechnology these sesquioxides materials are very attractive for their peculiar physical properties. From the beginning of RE technology, RE systems research were in focused by different experts to discover many fascinating characteristics. There are so many important applications of RE oxides and sesquioxides as catalysis and are enormously important materials in field of RE [1]. In spite of the fact that voluntarily oxidized RE elements, they appeared through their fluctuating strength [2]. For appropriate conditions the RE oxides from neodymium (Nd) onward (except Tb) arise naturally as sesquioxides RE_2O_3, and RE atoms are found in the trivalent (RE^{3+}) configuration in their ground state [3]. It has been found that the RE sesquioxides (RES) of wide-gap are translucent in the visible region [4]. In case of RES, the stalwartly electronegative oxygen ions are subsidized with three electrons by the rare earth atom and at the site of rare earth, residual 4f electrons powerfully are restricted. Whereas in case of lightweight lanthanides, the f electrons are comparatively loosely bounded, therefore it shows a greater number of oxygen coordination in case of compounds. RES shows many strange physical properties as conduction or valence electrons are interacting with confined 4f electrons [5–7]. RES has also been examined for their high permittivity performances, specifically as gate material insulators [8]. Considering the electronic properties, RES is very convenient for both scientists and technologists. Presently, density functional theory (DFT) based calculations in electronic structure has considered as a very fruitful way for explaining electronic properties of travelling valence electrons in solid-state structures. In the field of condensed-matter physics first-principles calculations of *f*-electron systems are of great challenges for the presence of localized as well as current theoretical methods based itinerant states, particularly in the local-density or generalized gradient approximation [9]. The optical properties based on optical phonon structure of RES are found in different literatures [10–14]. The analytical escalation and elemental properties such as density of states, band structures are main focused areas for theoretical and computational investigations on RES [15–17]. Recently, due to its extensive range of applications, neodymium sesquioxide (NDO) has drawn more attention to the several researchers in this modern era. NDO has vast applications in ceramic capacitors, high temperature coatings, carbon-sweep-light electrodes, vacuum depositions and in solid-state lasers [18]. By doping appropriate transition metal (TM) ions, we can manipulate charge and spin degrees of freedom in a single material. Also, currently investigation on laser optical amplifier, worked on electronic transition of RE ion has drawn attention of a group of researchers in the fabrication of metal ions doped RE materials. Even though several report on calculation of electronic structure, yet there are lot of gaps for the proper calculations on the electronic properties of TM substituted NDO. In this work we report a detail DFT calculation of TM doped rare earth neodymium sesquioxide (Nd_2XO_3, where X = Co, Cr, Mn, Ni and Zn) using Quantum-ESPRESSO (QE). A lot of interesting results were found from analysis of band structure calculations, density of states, projected and partial density of states, spin polarized magnetic properties and also from optical properties. Our results point out the main factors responsible for the enhanced magnetic properties, namely geometric and ionic contributions due to substitution of TM. Finally, we have addressed the way how TM substitutions contribute for tuning the desired electronic as well as optical properties.

2. Computational Method

Here in the present investigation of TM substitution in Nd_2O_3, we have used DFT in the pseudopotential formalism as executed in QE package [19, 20]. Ultrasoft pseudopotentials have been accustomed to demonstrate the connections between valence electrons and nuclei [21]. The generalized gradient approximation (GGA) is hired for the approximation between the exchange-correlation potential and the Perdew–Burke–Ernzerhof (PBE) exchange correlation functional [22]. It is very familiar that RES crystallizes in three different structures with space group such as hexagonal structure $P6_3/mmm$, monoclinic structure C2/m, and cubic structure Ia3. Here in the present work RES Nd_2O_3 crystallizes in the hexagonal structure [23]. The RE atoms are found be positioned at 2d sites $\pm(\frac{1}{3}, \frac{2}{3}, u)$, one oxygen (O) atom at 1a site (0,0,0) and the other two O atoms at 2d sites $\pm(\frac{1}{3}, \frac{2}{3}, v)$ [7]. Here it is to be mentioned that, this cell comprising formula units as a 1 × 1 × 1 cell of Nd_2O_3, which contains a total of 5 atoms. The calculated equilibrium lattice parameters are: a=5.82987 Å, b=5.82987 Å, c=3.02702 Å, which are in very good agreement with the other literature surveys [1, 7, 18]. For this present work we have used 1 × 1 × 2

supercell, with a Monkhorst–Pack k-mesh of 4 × 4 × 4. TM substitution effects are exhibited by means of periodic repetition of supercells of 1 × 1 × 2 covering 10 atoms, with the reduction of number of k-points in accordance with the modeled supercell. For calculations a plane wave cutoff of 60 Ry was used everywhere. In the calculations of convergence threshold of 10^{-9} Ry was done by using the Davidson diagonalization algorithm [24]. With the help of Broyden-Fletcher-Goldfarb-Shanno (BFGS) algorithm, relaxation of the structures [25], variable cell relaxation to a pressure convergence threshold of 0.5 kBar was done and with Hellmann-Feynman forces reduced to less than 10^{-4} Ry/Bohr. The optical properties of pure and doped NDO samples were measured by using random phase approximation (RPA) approach, as executed in the epsilon.x toolset [26]. The joint density of states (JDOS) is well-defined as [26, 27],

$$J(\omega) = \sum_{n} \sum_{n'} \frac{V}{(2\pi)^3} \int d^3k \delta(E_{k,n'} - E_{k,n} - \hbar\omega) \ldots \left[f\left(E_{k,n}\right) - f\left(E_{k,n'}\right) \right]$$

1

where, V is the volume of the lattice cell, δ is the spin component, n, n' belong respectively to conduction and valence bands, $E_{k,n}$ are the eigenvalues of the Hamiltonian and $f(E_{k,n})$ is the Fermi distribution function due to the occupation of the bands. The Dirac delta function is approached by a Gaussian distribution, normalized to one [26, 27],

$$G(\omega) = \frac{1}{\Gamma\sqrt{\pi}} exp\left\{ \frac{\left(E_{k,n'} - E_{k,n} - \hbar\omega\right)^2}{\Gamma^2} \right\}$$

2

where, Γ is the broadening parameter. The real part of dielectric function originates from the Kramers-Kronig transformation [26],

$$\epsilon_{1_{\alpha\beta}}(\omega) = 1 - \frac{4\pi e^2}{VN_k m^2} \sum_{n,k} \frac{df\left(E_{k,n}\right)}{dE_{k,n}} \frac{\omega^2 \hat{M}_{\alpha,\beta}}{\omega^4 + \eta^2\omega^2} + \cdots + \frac{8\pi e^2}{VN_k m^2} \sum_{n \neq n'} \sum_{k} \frac{\hat{M}_{\alpha,\beta}}{\left(E_{k,n'} - E_{k,n}\right)} \cdots \frac{\left[\left(\omega_{k,n'} - \omega_{k,n}\right)^2 - \omega^2\right] f\left(E_{k,n}\right)}{\left[\left(\omega_{k,n'} - \omega_{k,n}\right)^2 - \omega^2\right]^2 + \Gamma^2\omega^2}$$

3

The complex dielectric function is given by [26, 27],

$$\epsilon_{2_{\alpha\beta}}(\omega) = 1 - \frac{4\pi e^2}{VN_k m^2} \sum_{n,k} \frac{df\left(E_{k,n}\right)}{dE_{k,n}} \frac{\hat{M}_{\alpha,\beta}}{\omega^2 + i\eta\omega} + \cdots + \frac{8\pi e^2}{VN_k m^2} \sum_{n \neq n'} \sum_{k} \frac{\hat{M}_{\alpha,\beta}}{\left(E_{k,n'} - E_{k,n}\right)} \cdots \frac{f\left(E_{k,n}\right)}{\left(\omega_{k,n'} - \omega_{k,n}\right)^2 + \omega^2 + i\Gamma\omega}$$

4

where, η and Γ are respectively the inter-band and intra-band smearing. The square matrix element $\hat{M}_{\alpha,\beta}$ are defined as,

$$\hat{M}_{\alpha,\beta} = \langle u_{k,n'} | \hat{p}_\alpha | u_{k,n} \rangle \langle u_{k,n} | \hat{p}_\beta^\dagger | u_{k,n'} \rangle$$

5

By applying London transformation upon $\epsilon_{2_{\alpha\beta}}(\omega)$, we can get the dielectric tensor calculated on the imaginary frequency axis may be written as [26, 27],

$$\epsilon_{\alpha,\beta}(i\omega) = 1 + \frac{2}{\pi} \int_0^\infty \frac{\omega' \epsilon_{2_{\alpha\beta}}\left(\omega'\right)}{\left(\omega'^2 + \omega^2\right)} d\omega'$$

6

Taking consideration of the imaginary part of the inverse dielectric tensor, energy loss spectrum (theoretical EELS count) is calculated [27].

Different optical parameters such as refractive index n(ω), absorption coefficient α(ω), extinction coefficient k(ω), reflectivity spectrum R(ω) of all TM doped NDO samples can be derived from real and imaginary part of dielectric constants [28–31].

$$n(\omega) = \left[\sqrt{\varepsilon_1^2(\omega) + \varepsilon_2^2(\omega)} + \varepsilon_1(\omega)\right]^{1/2} / \sqrt{2} \quad (7)$$

$$\alpha(\omega) = \sqrt{2}\omega \left[\sqrt{\varepsilon_1^2(\omega) + \varepsilon_2^2(\omega)} - \varepsilon_1(\omega)\right]^{1/2} \quad (8)$$

$$k(\omega) = \frac{\alpha(\omega)}{2\omega}$$

9

$$R(\omega) = \frac{(n-1)^2 + k^2}{(n+1)^2 + k^2}$$

10

3. Results And Discussion

3.1 Crystal structures and Charge density distribution

Using QE, we have explored the properties of TM doped NDO on the structural, electronic, magnetic and optical background. All the optimized structures were shown in a hexagonal 1 × 1 × 2 supercell (Fig. 1) of 2 formula units of NDO and entire 10 atoms were first found by lowering the ground state energy. 25% doping was detected by replacing a Nd atom with a TM atom (Co, Cr, Mn, Ni, and Zn) in the supercell (as shown in Fig. 1 (a)–(f)). Table 1 presents the lattice parameters, cell volumes, bond lengths and bond angles of the optimized structural parameters of pristine NDO and all doped samples. We have found the reduction of volume of the supercell keeping crystal systems unchanged after replacing one Nd with any one of Co, Cr, Mn, Ni, Zn atom. The volume change may be instigated by the smaller ionic radii of Co (0.74Å), Cr (0.80Å), Mn (0.67Å), Ni (0.69Å) and Zn (0.70Å) with that of Nd (0.98Å). When X (Co, Cr, Mn, Ni, and Zn) elements were incorporated to NDO, all crystal systems remain hexagonal, while the volumes changes become clearly visible. For Mn, Ni and Zn doped NDO, the volumes shrink noticeably. It can be related for the reduction of lattice parameter and markedly different hexagonal angles in these three doped samples. Nevertheless, the volumes for Co and Cr doped NDO display slight upsurge compared with Mn, Ni and Zn doped NDO, which is due to slight difference between the sizes of ionic radii. It is already been established that a change in crystal structures [32], plays a key role to magnetic interaction, therefore the magnetic properties of each doped samples are used for additional investigation.

Table 1 The lattice constants (a, 2c), cell volumes, Nd–O bond lengths, and Nd–O–Nd bond angles of optimized NDO, NDCoO, NDCrO, NDMnO, NDNiO, and NDZnO structures.

Samples	Lattice parameters (Å)		Volume $(Å)^3$	Bond length, Nd–O (Å)	Bond angle, Nd–O–Nd (degree)
	a	2c			
NDO	5.82987	6.05403	211.08307	2.2634	83.9317
NDCoO	5.80448	5.96108	206.93765	2.2409	83.6624
NDCrO	5.80483	5.96135	206.95967	2.2389	83.7332
NDMnO	5.77310	5.90312	203.81757	2.2236	83.3277
NDNiO	5.77412	5.91242	204.17499	2.2258	83.2704
NDZnO	5.77978	5.92936	204.96092	2.2303	83.2782

To get a clear picture about the electric properties of pure NDO and TM doped NDO, charge density distribution (CDD) were shown in Fig. 2(a)–(f), furthermore electron localization function (ELF) are shown in Fig. 3(a)–(f) along (101) crystallographic plane. In Fig. 3. we have noticed gaining of electrons and losing of electrons respectively near the yellowish area around different O^{2-} ions and the greenish/blueish area around Nd^{3+}/TM ions. For TM doped samples if we consider the relative electronegativities and charge transfer among the different O and Nd/TM atoms, we have observed an interesting fact that electron density of the bonding electron pair partially was nearer to one of the bounded nuclei, which ultimately creates fractionally positive and negative atomic centers. We have further observed from both CDD and

ELF that there was a slight asymmetry in Nd–O bonds with partially finite covalency. Further noticeable asymmetric nature was observed in NDCoO and there was an improvement of ionic character in Co–O bonds. From Fig. 3 we have seen that due to the extra electrons gathering around Co^{2+} Cr^{2+}, and Mn^{2+} which suggests greater ionic characteristics in Co–O, Cr–O and Mn–O bonds than Nd–O bond. After substitution of TM into NDO, there might be a transmission of the bonded electrons from one atom to another ensuing an ionic bond and consequent positive and negative charged ions are attracted by electrostatic force. For NDNiO, number of nearest electrons of Nd^{3+} reduce and number of nearest electrons of Ni^{2+} upsurge a little, causing an intensification of ionic character for Ni-O bonds. In case of NDZnO, the electrons are in different concentration around Nd^{3+} and Zn^{2+}. In case of metals, we might notice that individually atom delivers one or more number of electrons which exist in atomic centers creating delocalized bonding electrons and therefore, a lot of interesting phenomena like electrical conductivity and thermal conductivity may occur due to the random motion of the delocalized electrons [33].

3.2 Energy bands structure, Density of States, and Magnetic properties

Our calculations for band structures laterally the more regularity direction in the Brillouin zone were shown in Fig. 4 (a)–(f). As shown in Table 2, the band gap (E_g) of NDO of 3.865 eV, which is similar with respect to the previously conveyed articles [1, 7, 14, 18, 34–37]. The calculated band gaps for other doped samples are shown in Table 2. It is clear that band gap has been reduced, i.e., the band gap shows less reduction rate due to substituting of transition element in pristine NDO. The changes detected here might occur in the bonding environment due to TM doping, which ultimately results in the lowering of lattice symmetry. Energy bands of pure NDO and other TM substituted samples are of two parts, one for the upper the Fermi energy (E_F) which is denser than current lower portion of E_F and other is below the Fermi level which is primarily due to the O atom, alongside a minor influence of Nd. However, the energy bands above Fermi level, due to Nd atom was observed and influence of O atom above the E_F is nearly insignificant. This can also be seen from the Density of States (DOS) of all the samples. In the energy bands an indirect band gap between the L-A points was detected.

Table 2 Fermi energy, the total magnetic moment and band gap of NDO, NDCoO, NDCrO, NDMnO, NDNiO, and NDZnO.

Samples	Fermi energy, (eV)	Total magnetic moment, M_{total} (μB)	Band gap, E_g (eV)		
			This Work	Other Theoretical works	Other Experimental works
NDO	8.3060	0.00	3.865	3.58[a] 3.80[b] 3.57[c] 3.69[d] 4.65[e] 5.09[f]	4.70[g] 4.80[h]
NDCoO	7.0831	4.14	3.452		
NDCrO	7.6946	3.00	2.525		
NDMnO	7.6354	4.00	3.230		
NDNiO	6.9541	2.90	3.575		
NDZnO	6.3723	0.10	3.658		

[a]Reference 1, [b]Reference 7, [c]Reference 18, [d]Reference 30, [e]Reference 31, [f]Reference 32, [g]Reference 14, [h]Reference 33.

The spin-polarized DOS, total DOS and the expected density of states (PDOS) for individual atoms for NDO, NDCoO, NDCrO, NDMnO, NDNiO, and NDZnO were shown in different Figs. 5-9. DOS are testified for spin-up and spin-down electrons with respect to the central horizontal line, respectively (Fig. 5). Here the overlapping of O p, Nd s, Nd p, Nd d and X (where, X= Co, Cr, Mn, Ni, Zn) 3d electrons in doped NDO deliver the indication for interaction between them. It was perceived that most prominent peaks seemed in the energy region of −1 ∼ −4eV and from 5 ∼ 12eV for X (where, X= Co, Cr, Mn, Ni, Zn) doped NDO. Investigations from PDOS, the peaks are composed of O s, O p, Nd s, Nd p, Nd d and TM 3d electrons. The variable density of states for each orbit electrons can be ascribed to holes and electrons presented by doping of transition elements, as in case of Co, Cr, Mn and Ni there are more valance electrons than Nd. For TM substituted NDO, some states credited

by Co, Cr, Mn, Ni, Zn 3d states, appear in the energy region of −5 ∼ 2.5eV. If we compare with the PDOS of all doped samples in Fig. 6, we can find out that Nd p states and O p states suffer some changes when introducing TM atoms into NDO. The PDOS of all individual atomic orbitals for all the samples were shown in Fig. 7(a)−(f). The projected density of states of Nd 5d orbitals of NDO and doped NDO samples were shown in Fig. 8 (a)-(f). Whereas the projected density of states of Co, Cr, Mn, Ni and Zn 3d orbitals of TM doped NDO were shown in Fig. 9 (a)-(e). These figures suggest that the Nd 5d, Co, Cr, Mn, Ni and Zn 3d states get divided into t_{2g} (d_{xy}, d_{yz}, d_{xz}) and e_g (d_{z^2}, $d_{x^2-y^2}$) manifolds. In the presence of asymmetrical field, splitting of the d orbitals occurs depending upon the nature of the crystal field. In the up-spin channel, Nd d_{xy}, d_{yz}, d_{xz}, d_{z^2}, $d_{x^2-y^2}$ states lie from 1.27 to 12.91 eV in the conduction band for NDO (Fig. 8), while for doped samples d_{xy}, d_{yz}, d_{xz}, d_{z^2}, $d_{x^2-y^2}$ states lie from 2.65 to 12.44 eV for NDCoO, from 2.20 to 11.59 eV for NDCrO, from 2.47 to 11.95 eV for NDMnO, from 2.82 to 12.58 eV for NDNiO, and from 3.25 to 12.72 eV for NDZnO in the conduction band.

The calculated DOS for both spin up and spin down are observed to be asymmetric here and therefore give rise to an enhanced magnetic moment in TM doped NDO structures as shown in Fig. 6. The changes of Co, Cr, Mn, Ni and Zn 3d states (Fig. 9.) may result in change of total magnetic moment for doped samples. The total magnetic moment (M_{total}) of all the samples were shown in Table 2. Interestingly, we have seen an enhancement in net magnetic moments for all five TM atoms (Co, Cr, Mn, Ni, Zn) substituted NDO samples and which are 4.14μB (Co doped), 3.00μB (Cr doped), 4.00μB (Mn doped), 2.90μB (Ni doped) and 0.10μB (Zn doped) respectively. To explain the mechanism of magnetism in each TM atom doped NDO sample we have calculated Nd–O–Nd bond angles (shown in Table 1), and ultimately which plays a leading role in controlling the magnetism. We have noticed that Nd–O–Nd bond angles are not equal for all doped samples. Compared with the pristine NDO, we have observed that Nd–O–Nd bond angle changes with small variation after one Nd atom is being replaced by each of these transition Co, Cr, Mn, Ni, Zn atoms. However, when TM ions are introduced into NDO, the Nd–O–Nd bond angles decrease clearly. This Nd–O–Nd bond angle is not only having a vital role to control the orbital overlap between Nd and O atoms but also plays a great role in imposing the strength of magnetic exchange interaction in TM doped Nd_2O_3. This antiferromagnetic nature in TM substituted NDO might be due to a strong superexchange interaction of Nd^{3+} ions via O^{2-} ions [38, 39]. When we substitute Co^{2+}, Cr^{2+}, Mn^{2+}, Ni^{2+} and Zn^{2+} ions in place of Nd^{3+}, effective sizes of Nd-O bond length also decrease due to the smaller ionic sizes of these TM ions, which might cause a net enhancement of magnetic moments.

There was another explanation of magnetic interactions from the Anderson's Theory, which was based upon the two superexchange interactions, kinetic exchange and potential exchange [40]. Antiferromagnetic structure was developed when there was kinetic exchange between e_g electrons, created due to fraternization of the ligand-field orbitals with 180° metal–oxygen–metal bond. Whereas ferromagnetic structure was obtained when exchange of kinetic energy between t_{2g} electrons, on account of the direct exchange interaction among ligand-field orbitals. There was a key role played by *dp*σ bonds for kinetic exchange but the potential exchange was resulted by rather weaker *dp*π interactions, consequently the kinetic exchange was substantially stronger than the potential exchange [41]. Here in TM doped NDO samples, we have observed an indirect exchange between neighboring Nd^{3+} ions, which was actually linked by kinetic exchange between e_g electrons, finally causes antiferromagnetic ordering in doped samples. After TM doped into NDO, the kinetic exchange between e_g electrons changed and NDO suffer additional distortion which might cause a further decrease in Nd–O–Nd bond angles as represented in Table 1. Consequently, $e_g - e_g$ coupling in doped NDO samples originates a strong antiferromagnetic superexchange interaction [32, 42], and was fragmented so that we get an improvement in magnetic ordering in TM doped NDO samples.

3.3 Optical properties

For the analysis of band structures of solids, optical spectrum and energy-loss of electron excitation spectrum have been extensively used as influential measurement techniques. Over a wide energy range, excitation spectrum was experimentally measured in the form of either reflectivity or electron energy-loss function, because most of the interbond transition oscillator strength has been fatigued during that energy region. It was therefore a regular practice to apply Kramers-Krönig dispersion relations to analyze observed data, considering several optical parameters likely, the real and imaginary portions of the dielectric constants, refractive index, extinction coefficient, absorption co-efficient, optical joint density of states and the oscillator strength integral [43]. Here in this work the measured optical joint density of states (JDOS) of the all the undoped and doped NDO structures were shown in Fig. 10(a)-(f). As JDOS is a pointer in the measurement of accessible states for photons which is interacting in optical emission or absorption procedure, which is restrained as most important part in the measurement of optical characteristics for sample material [27]. Under the rigorous investigations, at the sharpness of all peaks of all samples, JDOS has been found to change separately from their position as well as the number of peaks. Here, the number of sharper peaks in case of NDCoO, NDNiO, NDZnO more than NDO. The extension of JDOS peaks for NDCoO, NDZnO are in greater range and also in number. A cascade of small but precise peaks in the range 2-8eV for transition element doped NDO be more than those in pure NdO. Around the 2-4eV energy range, NDCoO, NDNiO, NDMnO, and NDNiO show more possibilities in transitions than NDO. Also, around a higher energy of 6-9.5eV, there

exists a significant difference in terms of the JDOS among the doped and undoped NDO samples. The TM doped NDO are characterized by a weighty enhance in the JDOS roundly 2-6eV energy range.

The real part of the complex dielectric function (ϵ_1) of all the undoped and doped NDO samples were shown in Fig. 11(a)-(f). The imaginary part of the complex dielectric function (ϵ_2) were shown in Fig. 12(a)-(f) with two in-plane components (*x* and *y*) and one out of plane (z) component. For all the samples, the *z*-component of ϵ_2 appears shifted as compared with the in-plane components. We have noticed a prominent shift in case of NDCoO, NDCrO, NDMnO and NDZnO. Taking into the consideration of position for in-plane characteristics, additional distinct peaks at lesser energies between 0-2eV was observed for TM substituted NDO than pure NDO. In the lower energy range, the peaks of NDCrO and NDMnO are more concentrated together. These results substantiate with the JDOS spectra deliberated in previous section. The barb in accessible states in Co, Cr, and Zn substituted NDO for transition around the 0-2eV, are also observed by the occurrence of a sturdier retort in this region by the TM substitution, as compared to pure NDO. Here it is to be noted that, the results discussed here are constructed on a random-phase approximation (RPA) process as defined by Benassi et. al. [26]. This application grounded on a multi-particle approach and suggests greater precision over simulations with the single particle dielectric tensor [27].

Due to inelastic interactions, electron energy-loss spectroscopy (EELS) becomes an important investigation of the electron energy embryonic distribution from a provided sample. An EELS spectrum covers an important information about the specimen atoms. In addition, we get their electronic structures, bond-states, nearest neighbors' distributions, coordination numbers, dielectric constants, and band gaps from EELS. Depending on the energy lost in different energy regions [44], the above characteristics are observed in different prepared samples. Here the theoretical EELS counts were depicted in Fig. 13(a)-(f), displayed the maxima for the NDO at 2.36, 2.66 and 3.15eV for the *x, y* and *z* components respectively. For NDCoO the *x, y* and *z* components respectively observed at 9.48, 9.77 and 9.87eV; for NDCrO 2.67eV, 2.32eV, and 3.16eV; for NDMnO 2.71eV, 2.53eV, and 3.60 eV; for NDNiO 2.69eV, 6.58eV, and 3.51 eV; for NDZnO 1.12eV, 1.15eV, and 1.53eV.

Furthermore, optical properties of pure and doped NDO samples are examined from the analysis of different parameters such as refractive index n(ω), absorption coefficient α(ω), extinction coefficient k(ω), reflectivity spectrum R(ω). Here from Fig. 14(a) for refractive index n(ω) we have noticed that the shape of the curves changes prominently after the incorporation of transitional metal atom into the pristine NDO. For undoped NDO the refractive index was 9.5 at 0.30 eV. Whereas in case of NDCoO n(ω) was 2.8 at 0.85 eV, for NDCrO n(ω) was 14.5 at 0.45 eV, for NDMnO n(ω) was 5.0 at 0.47 eV, for NDNiO n(ω) was 5.1 at 0.42 eV and for NDZnO n(ω) was 5.8 at 0.05 eV. We have seen that there has been a nice tuning of n(ω) between the energy range 0-3 eV and the value of n(ω) was decreased due substitution of transitional elements (Co, Mn, Ni, Zn) except Cr. Such kind of observation suggests that the doping of transitional atoms deliberately change the nature of refractive index, which may finally result to manipulate the desired optical properties in doped NDO samples. Fig. 14(b) shows the absorption coefficient α(ω) of all the samples. Form Fig. 14(b) we have noticed that the prominent peak for pure NDO was at 0.34 eV, while for NDCoO, NDCrO, NDMnO, NDNiO, and NDZnO respectively were at 0.42 eV, 0.46 eV, 0.78 eV, 2.03 eV and 0.73 eV, i.e., within the region of 0-2 eV. Thus, we might say that absorption peaks position and intensity change slightly when we introduced transitional elements inside pure NDO. The reflectivity spectrum R(ω) of undoped and doped samples was shown in Fig. 14(c), and from that particular figure we have detected that the shape and positions of the reflectivity curves changes significantly. The highest reflectivity peaks were situated between 1-3 eV region. The changes among the reflectivity's of doped NDO samples are very prominent than pure NDO. Fig. 14(d) shows the extinction coefficient k(ω) of all the samples. It was noticed that peaks of extinction coefficient for transitional atom doped NDO samples move towards low energy region compared with pure NDO, and the intensities are also stronger than pristine NDO. Therefore, we might have a good modulation of optical properties due to the incorporation of TM atoms inside of pure NDO.

4. Conclusions

In short, we have done a broad DFT analysis of the structural, electronic, magnetic and optical properties of TM substitution in neodymium sesquioxide structures, replacing a Nd atom by a TM (Co, Cr, Mn, Ni and Zn) atom. The electronic effect of various TM substitution in NDO has been studied computationally and enhancement of total magnetization has been detected in doped NDO structures with Co doping shows the maximum magnetization. The DOS and PDOS calculations of all the optimized structures recommend a $P6_3/mmm$ evenness in all samples and there is no severe change in the structure except the lattice parameters and cell volumes. The DOS calculations correspondingly specify the enhanced magnetic properties in all the doped samples. We have examined the fact that the optical parameters were remarkably influenced in low energy region due to transitional atoms substitution in pristine NDO system and it might be very effective for the modification and manipulation of optical as well as electronic properties in RE NDO for optoelectronic applications. Such a detailed theoretical analysis within DFT framework by using QE might be accommodating in the future experimental prospect of RE sesquioxides and their technical applications.

Declarations

Acknowledgments

Here I (corresponding author) wish to acknowledge Priyanka Banerjee, a researcher at Kazi Nazrul University, for her valuable suggestions and kind assistance to prepare the manuscript.

Data availability

The data that support the findings of this study are available from the corresponding author upon reasonable request.

Code availability

Quantum-ESPRESSO main inputs are available on request from the authors.

The authors declare that there are no conflicts of interest related to this article.

References

1. Petit L, Svane A, Szotek Z, Temmerman WM (2005) First-principles study of rare-earth oxides. Phys Rev B 72:205118. https://doi.org/10.1103/PhysRevB.72.205118
2. Holland-Moritz E (1992) Coexistence of valence fluctuating and stable Pr ions in Pr_6O_{11}.. Phys B: Condens Matter 89:285–288. https://doi.org/10.1007/BF01318158
3. Eyring L (1979) Handbook on the Physics and Chemistry of Rare Earths, Vol. 3, edited by Gschneider KA, Jr. and Eyring L (North-Holland, Amsterdam) p. 337
4. Adachi G, Imanaka N (1998) The Binary Rare Earth Oxides. Chem Rev (Washington DC) 98:1479–1514. https://doi.org/10.1021/cr940055h
5. Tanaka S, Ogasawara H, Okada K, Kotani A (1995) Theory of the 4d→2p X-Ray Emission Spectroscopy in Ce_2O_3. J Phys Soc Jpn 64:2225–2232. https://doi.org/10.1143/JPSJ.64.2225
6. Moewes A, Ederer DL, Grush MM, Callcott TA (1999) Probing electron correlation, charge transfer, and Coster-Kronig transitions at the 3d and 4d thresholds of Nd by resonant inelastic scattering. Phys Rev B 59:5452–5456. https://doi.org/10.1103/PhysRevB.59.5452
7. Singh N, Saini SM, Nautiyal T, Auluck S (2006) Electronic structure and optical properties of rare earth sesquioxides (R_2O_3, R=La, Pr, and Nd). J Appl Phys 100:083525–083530. https://doi.org/10.1063/1.2353267
8. Ohmi S, Kobayashi C, Kashiwagi I, Ohshima C, Ishiwara H, Iwai H (2003) Characterization of La_2O_3 and Yb_2O_3 Thin Films for High-k Gate Insulator Application. J Electrochem Soc 150:F134–F140. https://doi.org/10.1149/1.1581278
9. Jiang H, Rinke P, Scheffler M (2012) Electronic properties of lanthanide oxides from the GW perspective. Phys Rev B 86:125115–125113. https://doi.org/10.1103/PhysRevB.86.125115
10. McDevitt NT, Davidson AD (1966) Infrared Lattice Spectra of Cubic Rare Earth Oxides in the Region 700 to 50 cm^{-1}. J Opt Soc Am 56:636–638. https://doi.org/10.1364/JOSA.56.000636
11. Nigara Y (1968) Measurement of the Optical Constants of Yttrium Oxide. Jpn J Appl Phys 7:404–408. https://doi.org/10.1143/JJAP.7.404
12. Nigara Y, Ishigame M, Sakurai T (1971) Infrared Properties of Yttrium Oxide. J Phys Soc Jpn 30:453–458. https://doi.org/10.1143/JPSJ.30.453
13. Bloor D, Dean JR, Stedman GE (1970) Spectroscopic Observations of Antiferromagnetic Erbium Oxide. J Appl Phys 41:1242–1244. https://doi.org/10.1063/1.1658892
14. Prokofiev AV, Shelykh AI, Melekh BT (1996) Periodicity in the band gap variation of Ln_2X_3 (X = O, S, Se) in the lanthanide series. J Alloys Compd 242:41–44. https://doi.org/10.1016/0925-8388(96)02293-1
15. Koelling DD, Boring AM, Wood JH (1983) The electronic structure of CeO_2 and PrO_2. Solid State Commun 47:227–232. https://doi.org/10.1016/0038-1098(83)90550-1
16. Fabris S, de Gironcoli S, Baroni S, Vicario G, Balducci G (2005) Taming multiple valency with density functionals: A case study of defective ceria. Phys Rev B 71:041102–041104. https://doi.org/10.1103/PhysRevB.71.041102
17. Dabrowski J, Zavodinski V, Fleszar A (2001) Pseudopotential study of PrO_2 and HfO_2 in fluorite phase. Microelectron Reliab 41:1093–1096. https://doi.org/10.1016/S0026-2714(01)00070-1

18. Mohammad FM, Ghaleb AM, Jagrati S, Ahuja BL, Bhamu KC (2012) Investigation of electronic structure of Nd_2O_3: Experiment and theory. Natural Science 4:797–802. http://dx.doi.org/10.4236/ns.2012.410106
19. Giannozzi P et al (2009) QUANTUM ESPRESSO: a modular and open-source software project for quantum simulations of materials. J Phys: Condens Matter 21:395502–395520. https://doi.org/10.1088/0953-8984/21/39/395502
20. Giannozzi P et al (2017) Advanced capabilities for materials modelling with Quantum ESPRESSO. J Phys: Condens Matter 29:465901–465930. https://doi.org/10.1088/1361-648X/aa8f79
21. Vanderbilt D (1990) Soft self-consistent pseudopotentials in a generalized eigenvalue formalism. Phys Rev B 41:7892–7895. https://doi.org/10.1103/PhysRevB.41.7892
22. Perdew JP, Burke K, Ernzerhof M (1996) Generalized Gradient Approximation Made Simple. Phys Rev Lett 77:3865–3868. https://doi.org/10.1103/PhysRevLett.77.3865
23. Wyckoff RWG (1965) Crystal Structures, 2. Interscience, New York Vol
24. Davidson ER (1983) Methods in Computational Molecular Physics edited by Diercksen GHF and Wilson S Vol. 113 NATO Advanced Study Institute, Series C (Plenum, New York) p. 95
25. Head JD, Zerner MC (1985) A Broyden-Fletcher-Goldfarb-Shanno optimization procedure for molecular geometries. Chem Phys Lett 122:264–270. https://doi.org/10.1016/0009-2614(85)80574-1
26. Benassi A, Ferretti A, Cavazzoni C PWSCF. 's epsilon.x user's manual
27. Sengupta A (2019) Electronic and optical properties of SnX_2(X=S, Se) - InSe van der Waal's heterostructures from first-principle calculations. Phys Scr 94:125806. http://dx.doi.org/10.1088/1402-4896/ab3bb3
28. Saha S, Sinha TP, Mookerjee A (2000) Electronic structure, chemical bonding, and optical properties of paraelectric $BaTiO_3$. Phys Rev B 62:2805–2807. https://doi.org/10.1103/PhysRevB.62.8828
29. Li Y, Zhao X, Fan W (2011) Structural, Electronic, and Optical Properties of Ag-Doped ZnO Nanowires: First Principles Study. J Phys Chem C 155:3552–3557. https://doi.org/10.1021/jp1098816
30. Cazzaniga M, Caramella L, Manini N, Onida G (2010) Ab initio intraband contributions to the optical properties of metals. Phys Rev B 82:35104. https://doi.org/10.1103/PhysRevB.82.035104
31. Zhang H, Tao Z, Xu W, Lu S, Yuan F (2012) First-principles study of dopants and defects in S-doped ZnO and its effect on photocatalytic activity. Comput Mater Sci 58:119–124. https://doi.org/10.1016/j.commatsci.2012.01.016
32. Zhou Y et.al (2019) Effect of non-metallic X (X=F, N, S) and Cr co-doping on properties of $BiFeO_3$: A first-principles study. Phys Lett A 383:383–388. https://doi.org/10.1016/j.physleta.2018.10.045
33. Dračínský M (2017) Chapter One - The Chemical Bond: The Perspective of NMR Spectroscopy, Annual Reports on NMR Spectroscopy, 90:1-40. https://doi.org/10.1016/bs.arnmr.2016.07.001
34. Jiang H, Rinke P, Scheffler M (2012) Electronic properties of lanthanide oxides from the GW perspective. Phys Rev B 86:125115–125127. https://doi.org/10.1103/PhysRevB.86.125115
35. Gillen R, Clark SJ, Robertson J (2013) Nature of the electronic band gap in lanthanide oxides. Phys Rev B 87:125116–125121. https://doi.org/10.1103/PhysRevB.87.125116
36. El-Kelany Kh E, Ravoux C, Desmarais JK, Cortona P, Pan Y, Tse JS, Erba A (2018) Spin localization, magnetic ordering, and electronic properties of strongly correlated Ln_2O_3 sesquioxides (Ln=La, Ce, Pr, Nd). Phys Rev B 97:245118–245127. https://doi.org/10.1103/PhysRevB.97.245118
37. Kimura S, Arai F, Ikezawa M (2000) Optical Study on Electronic Structure of Rare-Earth Sesquioxides. J Phys Soc Jpn 69:3451–3457. https://doi.org/10.1143/JPSJ.69.3451
38. Majeed S, Shivashankar SA (2014) Rapid microwave-assisted synthesis of Gd_2O_3 and Eu:Gd_2O_3 nanocrystals: characterization, magnetic, optical and biological studies. J Mater Chem B 2:5585–5593. https://doi.org/10.1039/C4TB00763H
39. Patel SKS, Dhak P, Kim MK, Lee JH, Kim M, Kim SK, (2016) Structural and magnetic properties of Co-doped Gd_2O_3 nanorods. J. Mag. Mag. Mater. 403:155-160. https://doi.org/10.1016/j.jmmm.2015.11.093.
40. Anderson PW, Rado GT, Suhl H (eds) (1963) Magnetism, vol 1. Academic Press, New York, pp 25–83, Chap. 2
41. Baettig P, Ederer C, Spaldin NA, (2005) First principles study of the multiferroics $BiFeO_3$, Bi_2FeCrO_6, and $BiCrO_3$: Structure, polarization, and magnetic ordering temperature. Phys. Rev. B 72:214105-12 https://doi.org/10.1103/PhysRevB.72.214105.
42. Sun Y, Sun ZH, Wei R, (2018) First principles study of the magnetic properties and charge transfer of Ni-doped $BiFeO_3$. J. Magn. Magn. Mater. 449:10–16. https://doi.org/10.1016/j.jmmm.2017.09.063.

43. Liang WY, Beal AR, (1976) A study of the optical joint density of states function, J. Phys. C: Solid State Phys. 9:2823-2832. http://dx.doi.org/10.1088/0022-3719/9/14/020.
44. Hirai H (2003) Chapter 15 - Electron Energy-Loss Spectroscopy and its Applications to Characterization of Carbon Materials, Carbon Alloys, 239-256. https://doi.org/10.1016/B978-008044163-4/50015-2.

Figures

Figure 1

Structural models of (a) pristine NDO; transition metal doped NDO (b) NDCoO, (c) NDCrO, (d) NDMnO, (e) NDNiO, and (f) NDZnO.

Figure 2

Charge density distribution (CDD) of (a) NDO, (b) NDCoO, (c) NDCrO, (d) NDMnO, (e) NDNiO, and (f) NDZnO.

Figure 3

Electron localization function (ELF) of (a) NDO, (b) NDCoO, (c) NDCrO, (d) NDMnO, (e) NDNiO, and (f) NDZnO [Plotted using VESTA software].

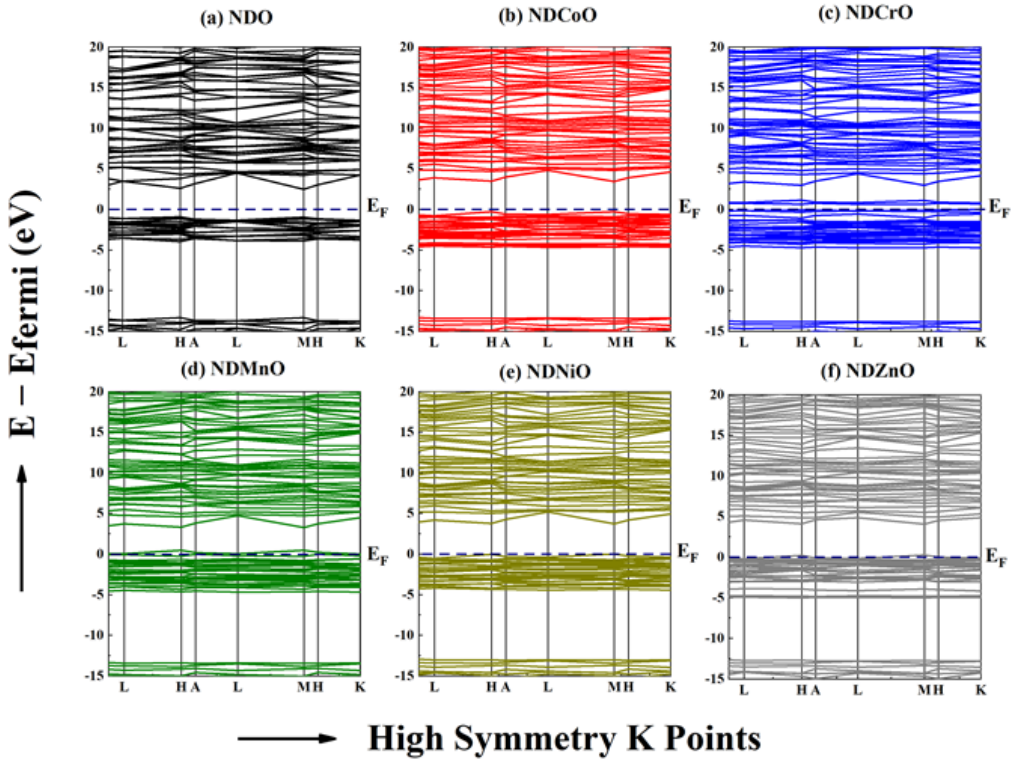

Figure 4

The comparative study of calculated electron band structure along the high symmetry K points in the Brillouin zone in (a) NDO, (b) NDCoO, (c) NDCrO, (d) NDMnO, (e) NDNiO, and (f) NDZnO.

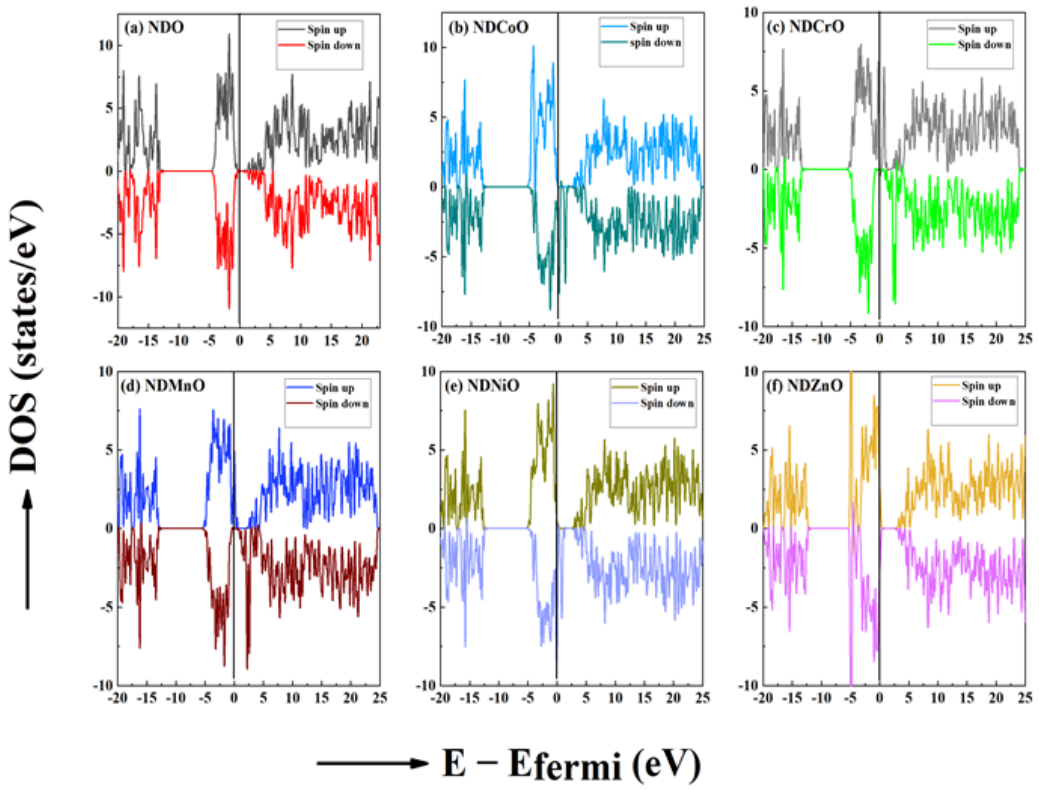

Figure 5

Calculated density of states (DOS) of undoped and transition metal doped NDO (a) NDO, (b) NDCoO, (c) NDCrO, (d) NDMnO, (e) NDNiO, and (f) NDZnO.

Figure 6

Total density of states (TDOS) and projected density of states (PDOS) of undoped and transition metal doped NDO 1×1×2 superlattice, (a) NDO, (b) NDCoO, (c) NDCrO, (d) NDMnO, (e) NDNiO, and (f) NDZnO.

Figure 7

PDOS (s, p, d - spin up and spin down) of (a) NDO, (b) NDCoO, (c) NDCrO, (d) NDMnO, (e) NDNiO, and (f) NDZnO.

Figure 9

See image above for figure legend.

Figure 10

The calculated joint density of states (JDOS) of (a) NDO, (b) NDCoO, (c) NDCrO, (d) NDMnO, (e) NDNiO, and (f) NDZnO.

Figure 11

The calculated real part of the complex dielectric function of (a) NDO, (b) NDCoO, (c) NDCrO, (d) NDMnO, (e) NDNiO, and (f) NDZnO.

Figure 12

The calculated imaginary part of the complex dielectric function of (a) NDO, (b) NDCoO, (c) NDCrO, (d) NDMnO, (e) NDNiO, and (f) NDZnO.

Figure 13

The electron energy loss spectra of (a) NDO, (b) NDCoO, (c) NDCrO, (d) NDMnO, (e) NDNiO, and (f) NDZnO.

Figure 14

The calculated optical parameters: (I) the refractive index n(ω), (II) the absorption coefficient α(ω), (III) the reflectivity spectrum R(ω), (IV) the extinction coefficient k(ω), of (a) NDO, (b) NDCoO, (c) NDCrO, (d) NDMnO, (e) NDNiO, and (f) NDZnO.

Supplementary Files

This is a list of supplementary files associated with this preprint. Click to download.

- Graphicalabstract.docx